Comparison of *Escherichia coli* surface attachment methods for single-cell, *in vivo* microscopy

Yao Kuan Wang[1, +], Ekaterina Krasnopeeva[2, +], Ssu-Yuan Lin[1], Fan Bai[3], Teuta Pilizota[2, *], and Chien-Jung Lo[1, *]

[1]Department of Physics and Graduate Institute of Biophysics, National Central University, Jhongli, Taiwan 32001, ROC
[2]Centre for Synthetic and Systems Biology, Institute of Cell Biology, School of Biological Sciences, University of Edinburgh, Alexander Crum Brown Road, EH9 3FF, Edinburgh, UK
[3]Biodynamic Optical Imaging Center (BIOPIC), School of Life Sciences, Peking University, Beijing 100871, China
[*]corresponding authors teuta.pilizota@ed.ac.uk, cjlo@phy.ncu.edu.tw
[+]these authors contributed equally to this work

ABSTRACT

For *in vivo*, single-cell imaging bacterial cells are commonly immobilised via physical confinement or surface attachment. Different surface attachment methods have been used both for atomic force and optical microscopy (including super resolution), and some have been reported to affect bacterial physiology. However, a systematic comparison of the effects these attachment methods have on the bacterial physiology is lacking. Here we present such a comparison for bacterium *Escherichia coli*, and assess the growth rate, size and intracellular pH of cells growing attached to different, commonly used, surfaces. We demonstrate that *E. coli* grow at the same rate, length and internal pH on all the tested surfaces when in the same growth medium. The result suggests that tested attachment methods can be used interchangeably when studying *E. coli* physiology.

Introduction

Microscopy has been a powerful tool for studying biological processes on the cellular level ever since the first discovery of microorganisms by Antonie van Leeuwenhoek back in 17th century[1]. Recently employed *in vivo* single-cell imaging allowed scientists to study population diversity[2], physiology[3], sub-cellular features[4], and protein dynamics[5] in real-time. Single cell imaging of bacteria is particularly dependent on immobilisation, as majority of bacteria are small in size and capable of swimming. Immobilisation methods vary depending on the application, but typically fall into one of the two categories: use of physical confinement or attachment to the surface via specific molecules. The former group includes microfluidic platforms capable of mechanical trapping[6,7], where some popular examples include the "mother machine"[8], CellASIC[9] or MACS[10] devices, and porous membranes such as agarose gel pads[2,11–13]. Physical confinement methods, while higher in throughout, can have drawbacks. For example, agarose gel pads do not allow fast medium exchange, and mechanically constrained bacteria cannot be used for studies of bacterial motility or energetics via detection of bacteria flagellar motor rotation[14–16]. Chemical attachment methods rely on the interaction of various adhesive molecules, deposited on the cover glass surface, with the cell itself. Adhesion can be a result of electrostatic (polyethylenimine (PEI)[17,18], poly-L-lysine (PLL)[14,16,18]) or covalent interactions (3-aminopropyltriethoxysilane (APTES)[18]), or a combination, such as with polyphenolic proteins (Cell-Tak^{TM})[18].

Time scales on which researchers perform single-cell experiments vary. For example, scanning methods, like atomic force microscopy (AFM) or confocal laser scanning microscopy (CLSM), require enough time to probe each point of the sample, and stochastic approaches of super resolution microscopy (e.g. PALM and STORM) use low activation rate of fluorophores to achieve a single fluorophore localisation. Thus, required acquisition time scales vary from milliseconds to minutes[19,20]. Experiments aimed at the observation of cell growth or slow cellular responses can run from minutes to hours[8,11,15,21,22].

Regardless of the time scale, physiology of the studied bacteria should not be affected by the surface attachment. For example, single particle tracking is often performed on surface immobilised cells[5,23,24], and cellular physiology can influence particle diffusion in the cytoplasm, e.g. metabolic "stirring" of the cytoplasm enhances diffusion in size dependant manner[25], and in yeasts an intracellular pH has been shown to affect cytoplasm fluidity[26]. Furthermore, concerns have been raised that charged molecules, like PLL that is commonly used for a surface attachment[16,22,23,27,28], can perturb membrane potential causing partial or complete membrane depolarisation[29,30]. Additionally, PLL in high concentrations exhibits antimicrobial properties[31]. Despite of these concerns, PLL has been widely used in super-resolution and single molecules tracking applications as it is cheap and easy to use[32,33]. It is, therefore, important to characterise physiological parameters on different surfaces, and

on the time scales relevant for live cell imaging.

In this report we compare a range of immobilisation techniques, including PLL, PEI, Cell-Tak^{TM} and agarose gel pad, using *Escherichia coli* as a model organism. We measure several physiological traits during growth on the specific surface, including growth rate, size and intracellular pH, and find that tested immobilisation methods do not differ; growth rate and cell size are surface-attachment independent.

Results

Immobilisation assays

We test four substrates commonly used for bacteria immobilisation: poly-L-lysine (PLL)[14,30], polyethylenimine (PEI)[17,34], Cell-Tak^{TM}[18], 3-aminopropyltriethoxysilane (APTES)[18] and agarose gel[20].

PLL and PEI are cationic polymers, which can electrostatically interact with negative charges on the outer surface of the cell[35]. Several PLL coating protocols have been reported, which we here refer to as "in-chamber"[14], "rinsed"[30], and "air-dried"[30] methods. "In-chamber" PLL coating is the most standard for bacterial flagellar motor experiments commonly known as bead assay[14,36–38]. In this protocol PLL solution is flushed into an uncoated glass flow-chamber for 10-15 s followed by thorough washing with the excessive volume of growth medium ($\sim$ 25 times the flow-chamber volume). In the "rinsed" method lower PLL concentration and longer incubation time (min) are used to cover the entire surface of the coverslip by immersing it in the PLL solution[30] amd subsequently washing. "Air-dried" method is similar to the "rinsed", with an addition of drying the PLL solution on the coated surface for over an hour. For our detailed coating protocols see *Materials and Methods*.

Cell-Tak^{TM} is a commercially available adhesive extracted from marine mussel, *Mytilus edulis*. It's a component of byssus, a bundle of filaments mussels secrete to anchor themselves to solid surfaces[39,40], where characterising and mimicking the adhesive chemistry of mussel byssus is an active area of research[41]. What we know from these efforts thus far, is that it involves bidentate and covalent interactions, protein coacervation, intrinsic protein-protein binding as well as metal chelation[41]. We use the manufacturer coating protocol as described in *Materials and Methods*.

APTES is a common choice for salinisation of microfluidic channels[42], and has also been employed as an attachment agent for the AFM imaging[18]. We coat coverslips by incubating them in a 2% solution of APTES for 2 h followed by extensive washing with water and acetone as described in *Materials and Methods*.

As a control we grow bacteria on the agarose gel pad with no chemical adhesives (see *Materials and Methods* for details).

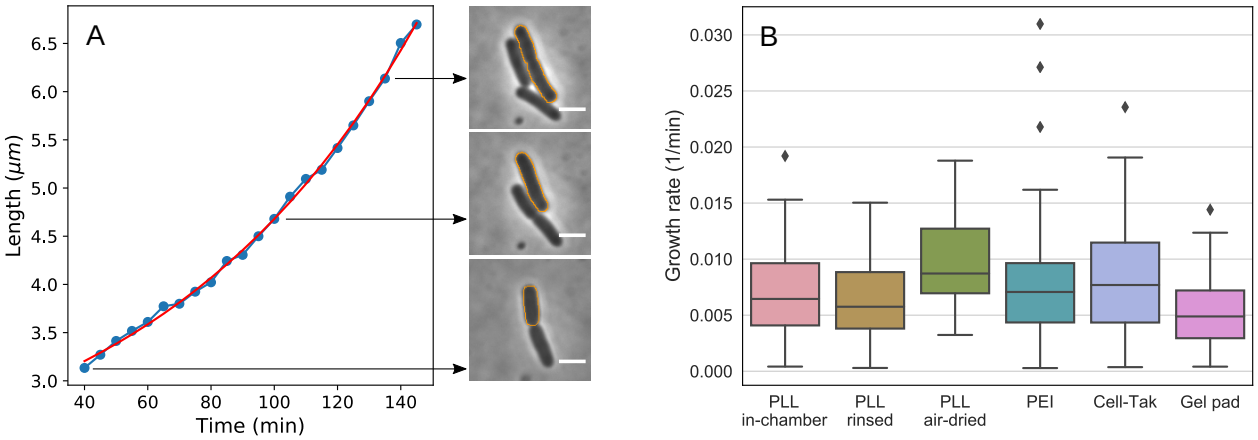

Figure 1. Bacterial growth rate stays constant when cells are attached to the surface with different attachment methods. (**A**) The single cell length is measured using phase contrast imaging over a complete cell cycle (from the first to the second division) and fitted with a single exponential function to obtain a single cell growth rate. Panel on the right show examples of the phase contrast images at the indicated time points. Scale bar is 2 μm. (**B**) Comparison of average growth rates on different surfaces shows no significant difference between all tested immobilisation methods in MM9 medium. The growth rates were measured at 23°C. Number of cells analysed for each attachment method is: N=44, 104, 28, 81, 48, and 43 for "PLL in-chamber", "PLL rinsed", "PLL air-dried", PEI, Cell-Tak and gel pad respectively.

Growth rate and morphology of bacteria do not dependent on the surface attachment method

To estimate the effect of different immobilisation assays on bacterial physiology we first examine the growth rate and the cells' morphology as the cells grow on each specific surface[8]. To obtain the growth rate and information on morphology we monitor bacteria between first and second divisions using optical microscopy (see *Materials and Methods*). Bacterial growth assays are performed at 23°C in the flow chambers, where fresh oxygenated medium is constantly supplied to the cells. Phase-contrast images of the bacteria are taken every 5 min and cells' length is extracted as described in *Materials and Methods* and Figure 1A. Figure 1B shows single cell growth rates, which we define as a rate of relative elongation of an exponentially growing bacterium[8,43], of the cells grown on different surfaces. The growth rate observed is independent on the surface attachment, and, when we average the values obtain for the 6 different surfaces in Figure 1B, equals (0.0071 ± 0.0044 min^{-1}) . As expected, the growth rate is medium dependant and becomes twice as high when we move from the MM9 medium (see *Materials and Methods*) to the richer LB medium (0.0153 ± 0.0049 min^{-1}), SI Figure 2A.

In addition to the growth rates, in Figure 2A we analyse the lengths of individual cells at the beginning and at the end of the growth cycle. Similarly to the growth rates, the initial (L_0) and final (L_f) length, and cell width (W) are maintained constant for different immobilisation methods: $L_0 = 2.61 \pm 0.31$µm in MM9 (Figure 2A) and 3.31 ± 0.54 µm in LB medium (SI Figure 2B), $L_f = 4.35 \pm 0.49$ µm in MM9 (Figure 2A inset) and 5.72 ± 0.95 µm in LB, and $W = 0.94 \pm 0.04$ µm in MM9 (Figure 2B), and 1.03 ± 0.07 µm in LB (SI Figure 2D). The length ratio (defined as the L_f/L_0) stays 1.69 ± 0.21, irrespective of the immobilisation method or the growth media (SI Figure 1).

Though independent of the immobilisation protocol, the length of the bacteria is sensitive to the surface attachment. When attached to a surface, average cell length grows smaller with time reaching a steady level already after the first division (SI Figure 3). The mean of the length distribution of surface-grown bacteria (after first division) is approximately 30% smaller than that of the planktonic cell population.

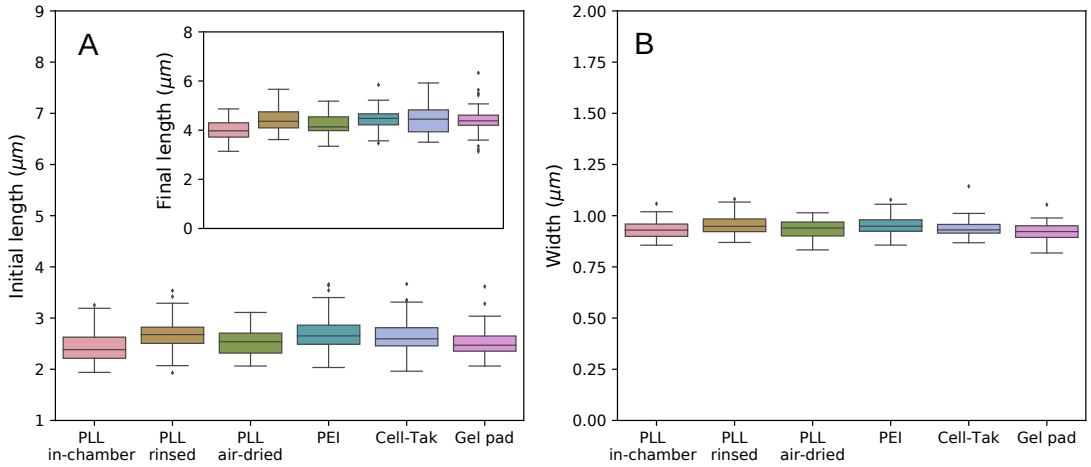

Figure 2. Morphology of bacteria is not influenced by the attachment method. (**A**) Initial cell length on different surfaces. Cells are grown in a bulk culture and immobilised on the surface. The length is measured after the first division following immobilisation. The inset shows the final cell length before the second division. (**B**) Width distribution of cells attached to the surface with various immobilisation methods remains constant.

Intracellular pH during growth on the surface does not depend on the method of attachment

Neutrophilic bacteria maintain their cytoplasmic pH withing a narrow range (termed pH homeostasis). For example, *E. coli* can survive in a range of external pHs, starting as low as pH ~ 2 in the human stomach and up to pH ~ 9 at the pancreatic duct, while maintaining internal pH in a relatively narrow range of 7-8[44–49]. Cytoplasmic pH plays an important role in cellular energetics as the difference between cytoplasmic and extracellular pH contributes to the electrochemical gradient of protons (so called proton motive force[50]), as well as influences protein stability and an enzymatic activity in the cell[51]. However, cytoplasmic pH can change when cells are subjected to an external stress, such as acid or osmotic shocks[48,52,53]. Furthermore, for some species acidification of the cytoplasm has been shown to be related to pathogenicity[54,55], and in yeast changes in the cytoplasmic pH affect particle cytoplasm[26]. Here we investigate if surface attachment methods influence the internal pH of bacteria during time lapse imaging.

To monitor the effect of the adhesive substances on the internal pH of *E. coli* cells during their growth on the coated surfaces, we use a genetically encoded indicator pHluorin[16,56,57]. pHluorin is a variant of the green fluorescent protein with pH sensitive spectrum that responds in a ratiometric manner, SI Figure 4. Prior to the growth experiments, pHluorin has been carefully calibrated both *in vivo* and *in vitro*, see *Supplementary Materials*[16]. For the *in vivo* calibration we've used various $\Delta pH = pH_{external} - pH_{internal}$ collapsing agents and noticed that the calibration curves deviate slightly depending on the uncoupler, which compromises the accuracy of the potential pH measurements. Though it is not clear what causes the difference in the calibration curves, we show that the combination of potassium benzoate and methylamine hydrochloride (PBMH) allows us to reproduce the *in vitro* calibration most accurately (SI Figure 5), and we subsequently use PBMH for *in vivo* calibration.

Having calibrated pHluorin, we measure the intracellular pH of the immobilised bacteria during growth and division tracking two generations, as shown in Figure 3. We find the average intracellular pH equals 8.39 ± 0.33 on all the tested surfaces at the beginning of experiments (this is the average pH value of the first 70 min in Figure 3A). For cells grown in MM9 the cytoplasmic pH decreases to 7.79 in an exponential-like manner over the course of several hours, thus we obtain the steady-state pH value by fitting all the pH traces in MM9 with exponential decay function. The intracellular pH drops mainly in the first generation and then remains costant with some cell to cell variation shown in SI Figure 6. In contrast, cytoplasmic pH of the cells growing in LB starts from 8.36 ± 0.06 and slightly increases within the two generations, SI Figure 7.

The intracellular pH values we measured are higher than those commonly found in the literature (7.2-7.8[47,48]). We assume these discrepancies originate from the fact that we constantly exchange the medium during the cell growth, removing from the environment metabolic waste products and any quorum sensing or signal molecules, which have been shown to influence cytoplasmic pH before[49,58,59]. Indeed, when cells are kept in the original growth medium their cytoplasmic pH varies between 7.3 and 7.7, Figure 3B. It, however, increases rapidly to 8.2-8.3 when fresh medium is supplied and can be reduced back to $\sim$7.8 upon the return to the original growth medium, Figure 3B. Further incubation in a fresh medium with no exchange (flow has been stopped) leads to the pH decrease to $\sim$ 7.5 after $\sim$ 10 min.

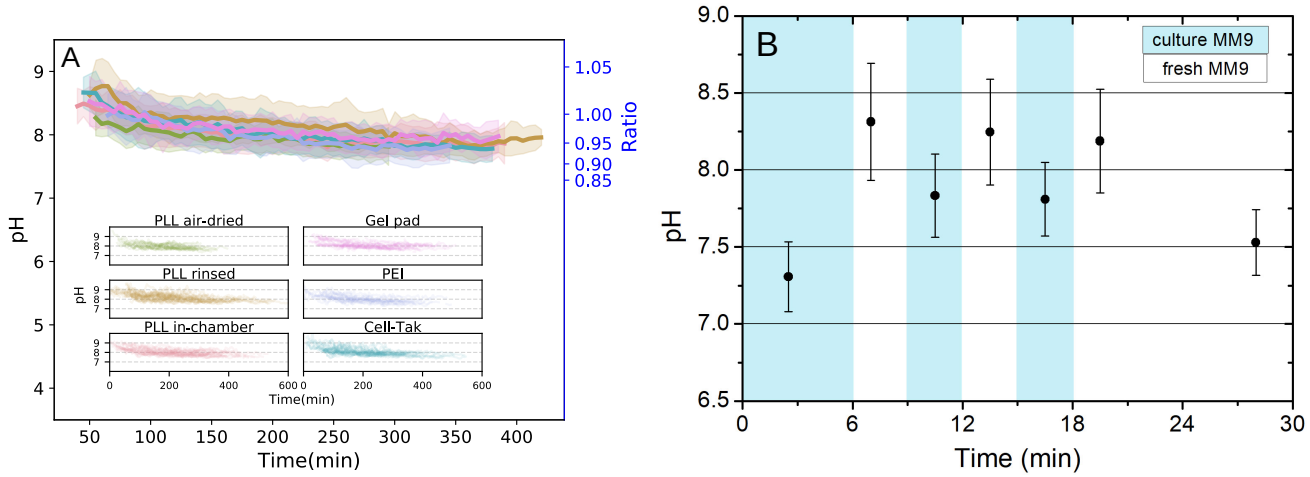

Figure 3. Intracellular pH dynamics of bacterial cells immobilised on a given surface. (**A**) Single cell intracellular pH is measured with cytoplasmic pHluorin during cell growth on different surfaces. Solid line and shaded area show the mean and standard deviation. All tested immobilisation methods exhibit similar tendencies: pH values start from pH 8.38 ± 0.29 and decrease to about pH 7.78 ± 0.16 within $\sim$7 h of observation. The inset shows all single-cell traces plotted for each condition. (**B**) Cells in a flow chamber are sequentially treated with the medium taken from a growing culture (blue regions) and fresh medium (white regions). Media exchange occurs in a short pulse manner at the beginning of each period, while no flow is applied during imaging. Data points show the mean of $N > 500$ measured bacteria with standard deviation as error bar.

Attachment quality on different surfaces varies

For single cell imaging it is important that analysed cells remain "flat"[22] (long axis parallel to the imaging plane) for the duration of observation, which could last several generations. Of the surfaces we have tested, "PLL in-chamber", "PLL rinsed", "PLL air-dried", PEI and Cell-Tak show similar attachment quality during cell growth and division. These surfaces also show consistent imaging quality under phase-contrast microscopy, Figure 4. Cells on the gel pad surface also remain 'flat', but we observe agarose impurities that influence image quality, Figure 4. Typical time lapse images can be done on these surfaces for

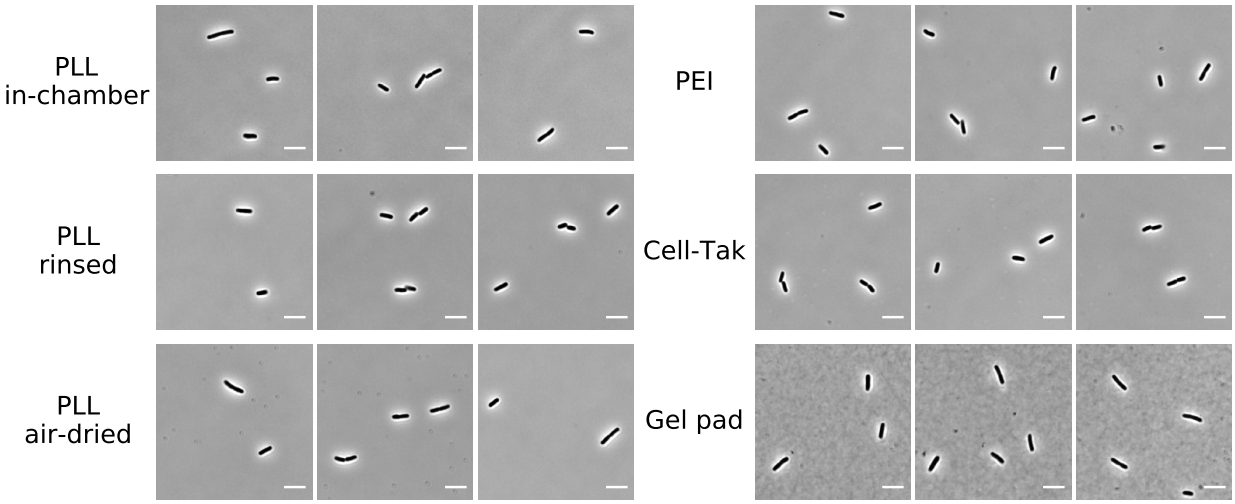

Figure 4. Examples of phase contrast images of *E. coli* cells attached to the surface with different immobilisation methods (scale bar is 5 µm). All images shows good "flatness" (see *Materials and Methods* for definition) and contrast for cell morphology tracking.

few generations. Covalent binding to APTES coated surface resulted in attached *E. coli* cells, however the cells usually detach during the cell growth leading to unsuccessful cell morphology tracking and pH measurements.

Discussion

Good surface attachment is an important requirement for bacterial single-cell studies using optical microscopy. However, we are unaware of a systematic study that characterises the effects on cells' physiology caused by different adhesives. Changes in the cellular physiology caused by different surface attachment methods can influence not only studies of cellular physiology themselves, but also studies focusing on specific cellular molecular mechanisms. For example, metabolic rate or internal pH could lead to the alteration of cytoplasm properties, e.g. its fluidity[25,26], and many intracellular processes, including DNA replication and cell division, are highly dependent on the growth rate[60,61]. It is, therefore, important to consider and characterise potential effects of the immobilisation method on physiology of the studied bacteria.

Here, we test a range of the immobilisation techniques and show that *E. coli*'s growth rate and shape are immobilisation method independent. Cell length and the growth rate are dependent on the growth medium, as expected, but independent of the surface attachment chemistry. Length ratio during the cell cycle (L_f/L_0) stays constant for all tested conditions, as has been previously noticed[62,63]. However, we see evidence of adaptation to the attachment to the surface itself, which is a relevant finding given the importance of understanding the physiology of surface-attached bacteria[64].

Interestingly, we notice that the cell size of bacteria growing on the surface is reduced compared to the free swimming bacteria, though it doesn't seem to be correlated with the attachment method. We speculate mechanosensing is involved to an extent, which could be further tested by using strains lacking pili and flagella (such as YD133[17]) that are known to be involved in surface sensing in bacteria[65].

Though the concerns regarding use of PLL for surface attachment have been previously expressed in the literature[29,66], we note that the experiments that demonstrate inhibition of cell division by PLL, do so for the case of free PLL molecules in the medium[30]. We show that all three of the tested PLL-coating protocols leave no residual PLL in the medium and do not influence bacterial growth rate and division.

For measurements of *E. coli*'s cytoplasmic pH we use pHluorin and find that *in vivo* calibration curve is dependant on the agents used to collapse pH. We do not understand the observations at present, but speculate that it could occur due to the interaction between the uncoupler (CCCP or indole) and the bacterium, e.g. CCCP can be actively exported by EmrAB-TolC pump[67]. Using pHluorin we show that the internal pH of the attached *E. coli* is kept between 7.3 and 8.4 and doesn't vary significantly with the surface coating. On all the tested surfaces in MM9 media the cytoplasmic pH decreases slightly (from

pH 8.38 to 7.78) in the course of the experiment, and the behaviour changes in LB medium, where cytoplasmic pH starts at pH 8.29 and increases over the observation time to pH 8.43. The result is not unexpected as metabolic byproducts have been demonstrated to influence *E. coli*'s cytoplasmic pH[49,58,68–71]. For example, glucose metabolism mainly produces organic acids as byproducts, such as acetate, lactate, formate, succinate etc.[68]. These organic acids are capable of crossing the inner membrane in their uncharged form dissociating in the cytoplasm, which causes full or partial collapse of the pH gradient across the membrane[49,58,69]. In the case of LB medium, the alkalinisation of the media due to *E. coli*'s metabolism has been reported and attributed to the release of the amine-containing compounds[70,71].

We, thus, conclude that all the tested bacteria immobilisation protocols can be used for live cells imaging without affecting cells' main physiological traits.

Materials and Methods

Bacterial Strains and Growth Conditions

The strain, EK03, is the *Escherichia coli* K-12 MG1655 strain with "sticky" flagella mutation[16,72] and pkk223-3/pHluorin(M153R) plasmid. The plasmid containing pHluorin with M153R mutation to have better stability of fusion proteins[56] was a kind gift from Dr. Tohru Minamino.

Cell cultures were inoculated in MM9 medium (Na_2HPO_4 50 mM, NaH_2PO_4 20 mM, NaCl 8.5 mM, NH_4Cl 20 mM, $CaCl_2$ 0.1 mM, KCl 1 mM, $MgSO_4$ 2 mM, 0.5% glucose , and MEM Amino acides solution (Gibco, USA) with 1:100 dilution from an overnight culture grown in Lysogeny broth (LB: 1% w/v Bacto-Tryptone, 0.5% w/v yeast extract and 0.5% w/v NaCl). Cultures are grown for 4 h at 37°C with continuous shaking (220 rpm) to reach optical density values between 0.4 and 0.5. The cells were further diluted 1:60 into MM9 or LB for the surface immobilisation protocols.

Microscope and Microfluidic chambers

Bacterial growth assays were conducted using a motorised, inverted optical microscope (Ti-E, Nikon, Japan) with perfect focus system for time lapse observation. The microscope is equipped with a 100x Objective (Plan Apo 100x/1.45NA lambda, Nikon, Japan), sCMOS Camera (Zyla 4.2, Andor, UK) and LED fluorescent excitation light source (PE4000, CoolLED, UK). Imaging was performed in phase-contrast and epifluorescence configuration, the latter was used for measuring the cytoplasmic pH with pHluorin. The exposure times for phase-contrast and epifluorescence imaging were 100 and 70 ms respectively, and images were recorded every 5 min. The excitation wavelengths imaging of pHluorin were 395 and 470 nm, achieved via a dual-band dichroic mirror (403/502nm, FF403/502-Di01-25x36, Semrock, USA) and a dual-band bandpass emission filter (FF01-433/530-25, Semrock, USA).

To supply fresh oxygenated media throughout the experiment we use a flow chamber made as follows. Two 1.5 mm holes were drilled in a microscope slide 20 mm apart. PTFE tubing with inner diameter 0.96 mm was attached to the slide with epoxy glue, SI Figure 8. The flow chamber was then created by attaching double sided tape or gene frame (Fisher Scientific, USA) to the slide and covering it with pre-coated or uncoated cover glass depending on the immobilisation protocol. Gene frame was used to create a larger chamber to fit the agarose pad, while sticky tape was used for all of the other protocols. Dimensions of the formed flow chamber are $3.5 \times 25 \times 0.2$ mm for doubled sided tape, and $17 \times 28 \times 0.25$ mm for gene frame. The flow chamber construction protocol varied slightly with different coating protocols. For the PLL "in chamber" and Cell-Tak coating methods, the flow chambers were sealed before coating. In other cases, the coverslips were coated prior to the flow chamber construction.

For all of the immobilisation assays medium was flown at 400 µl/min flow rate at the end of the attachment protocol for 4 min to remove poorly attached cells, upon which the the flow rate was altered to 4 µl/min for the duration of the experiment (12 h). Media was flown with a syringe pump (Fusion 4000, Chemyx, USA).

Immobilisation protocols

Preparation step: coverslip cleaning

The coverslip is sonicated in an ultrasonic bath with saturated solution of KOH in ethanol for 30 min. It is then rinsed with the deionised water and sonicated again. Glass treated this way does not allow cells attachment unless it's coated. The cleaning step has been performed prior to all attachment protocols.

PLL "in-chamber"

Surface of the flow chamber is coated with 0.1% poly-L-lysine (PLL) by flushing PLL through the channel for ∼10 s followed by washing it out with the excessive volume of growth medium (x20 times the volume of the chamber). Cells are then loaded into the flow chamber and incubated for 1 to 3 min to allow attachment, and then washed out as described under *Microscopy and Microfluidic chambers* section.

PLL "rinsed"

Coverslip is coated with the PLL prior to the flow chamber construction. 100 µl of the 0.01% PLL solution (diluted from P8920 Sigma-Aldrich, USA) is spread over approximate 1.5 cm^2 area. The solution is allowed to sit on the coverslip for 30 min, then washed off with 5 ml of deionised water. The coated coverslip is then used to construct a flow chamber. The cells are attached as above.

PLL "air-dried"

The protocol is similar to the "rinsed" method. Here, the PLL solution on the coverslip is air dried fully, typically for 1.5 h. The coated coverslip is then washed with 5 ml deionised water and used to construct a flow chamber. The cells are attached as above.

PEI

200 µl of 1% PEI is spread out on the coverslip covering the area the size of the flow chamber tunnel. Solution is incubated on the surface for 10 s, and washed off thoroughly with 100 ml of deionised water. The volume of the water should be much higher than that of the PEI to leave no residual PEI molecules that are not attached to the glass surface. Otherwise (e.g. if we use 5 ml of water), we observe cells blebbing[73,74] and dying when grown on the surface. We also notice that the "in-chamber" coating method is not applicable for PEI, as it leads to MM9 precipitation in the chamber caused by the leftover free PEI molecules. The cells are subsequently attached as described above.

Cell-Tak

Cell-Tak working mixture is prepared by adding 14 µl of Cell-Tak (1.16 mg/mL) to 174 µl $NaHCO_2$ (pH 8.0) followed by immediate vortexing. A pre-assembled flow chamber is incubated with Cell-Tak mixture for 20 min, then washed with 3 ml of deionised water. 3 ml of MM9 is flushed through the chamber before attaching the cells. Finally, cells are attached as above.

APTES

A coverslip was incubated in 2% APTES for 2 h, and then rinsed it with deionised water and acetone. The remaining acetone was air-dried with nitrogen. The coated coverslip was later used for the flow chamber construction. Cells are attached as above.

Agarose Gel Pad

For the agarose gel pad, the flow chamber area was 17×28 mm^2. The gel pad was created by adding a 5 µl droplet of melted 1% agarose to the middle of the flow chamber. 0.5 µl of the cell culture was added onto the solidified pad and covered with the coverslip. The fresh medium was constantly circulated around the agarose "island" during the experiment.

Image analysis

Cell segmentation

Phase contrast images of the cells were analysed with custom written Python script and ImageJ[75]. In phase microscopy, cells appear as dark objects on a light background, with a characteristic white halo, Figure 1 inset. Cells are segmented with Watershed algorithm[76,77] implemented as ImageJ Marker-controlled Watershed plugin[78]. The algorithm treats the image as a geological terrain. The lighter watershed which separates neighboring darker drainage basins is the edge around region of interest. After the segmentation, the cell length is calculated by PSICIC algorithm (Projected System of Internal Coordinates from Interpolated Contours)[79]. Briefly, the algorithm finds two poles of a cell as points that are the greatest Euclidean distance apart, thus creating two curves. On each of the two contour curves the algorithm evenly distributes equal number of points and then connects them (effectively creating width lines). Finally, the center line, i.e. the lenght of the cell, runs along the middle of the width lines[79].

Growth curve fitting

The growth of the cell follows $L = L_0 \times e^{bt} + c$, where L_0 is the cell length at the start of the recording, t time in minutes, b the growth rate, and c the constant representing the length of non-growing poles. The equation is fitted to the cell length using Levenberg-Marquardt algorithm[80], a non-linear least squares method, implemented using Scipy, a numerical package in Python[81]. Initial parameters we identified by first fitting a polynomial to the logarithmic growth of the cell length.

References

1. Dobell, C. *Antony van Leeuwenhoek and his "Little animals"* (Harcourt, Brace and company, 1932).
2. Elowitz, M. B., Levine, A. J., Siggia, E. D. & Swain, P. S. Stochastic Gene Expression in a Single Cell. *Sci. (80-.).* **297**, 1183–1186 (2002).

3. Taheri-Araghi, S., Brown, S. D., Sauls, J. T., McIntosh, D. B. & Jun, S. Single-Cell Physiology. *Annu. Rev. Biophys.* **44**, 123–142 (2015). DOI 10.1146/annurev-biophys-060414-034236. arXiv:1011.1669v3.

4. Raskin, D. M. & de Boer, P. A. J. Rapid pole-to-pole oscillation of a protein required for directing division to the middle of Escherichia coli. *Proc. Natl. Acad. Sci.* **96**, 4971–4976 (1999). DOI 10.1073/pnas.96.9.4971.

5. Ghodke, H., Ho, H. & van Oijen, A. M. Single-molecule live-cell imaging of bacterial DNA repair and damage tolerance. *Biochem. Soc. Trans.* **46**, 23–35 (2018). DOI 10.1042/BST20170055.

6. Hol, F. J. H. & Dekker, C. Zooming in to see the bigger picture: Microfluidic and nanofabrication tools to study bacteria. *Sci. (80-.).* **346** (2014).

7. Leygeber, M. *et al.* Analyzing microbial population heterogeneity - expanding the toolbox of microfluidic single-cell cultivations. *J. Mol. Biol.* (2019). URL http://www.sciencedirect.com/science/article/pii/S0022283619302323. DOI https://doi.org/10.1016/j.jmb.2019.04.025.

8. Wang, P. *et al.* Robust Growth of Escherichia coli. *Curr. Biol.* **20**, 1099–1103 (2010).

9. Humphries, J. *et al.* Species-Independent Attraction to Biofilms through Electrical Signaling. *Cell* **168**, 200–209.e12 (2017). DOI 10.1016/j.cell.2016.12.014.

10. Okumus, B. *et al.* Single-cell microscopy of suspension cultures using a microfluidics-assisted cell screening platform. *Nat. Protoc.* **13**, 170–194 (2018). DOI 10.1038/nprot.2017.127.

11. Hadizadeh Yazdi, N., Guet, C. C., Johnson, R. C. & Marko, J. F. Variation of the folding and dynamics of the Escherichia coli chromosome with growth conditions. *Mol. Microbiol.* **86**, 1318–1333 (2012). URL http://www.ncbi.nlm.nih.gov/pubmed/23078205http://www.pubmedcentral.nih.gov/articlerender.fcgi?artid=PMC3524407. DOI 10.1111/mmi.12071.

12. Moffitt, J. R., Lee, J. B. & Cluzel, P. The single-cell chemostat: An agarose-based, microfluidic device for high-throughput, single-cell studies of bacteria and bacterial communities. *Lab Chip* **12**, 1487–1494 (2012). URL http://www.ncbi.nlm.nih.gov/pubmed/22395180http://www.pubmedcentral.nih.gov/articlerender.fcgi?artid=PMC3646658. DOI 10.1039/c2lc00009a.

13. Priest, D. G., Tanaka, N., Tanaka, Y. & Taniguchi, Y. Micro-patterned agarose gel devices for single-cell high-throughput microscopy of E. coli cells. *Sci. Rep.* **7**, 17750 (2017). DOI 10.1038/s41598-017-17544-2.

14. Lo, C.-J., Sowa, Y., Pilizota, T. & Berry, R. M. Mechanism and kinetics of a sodium-driven bacterial flagellar motor. *Proc. Natl. Acad. Sci. U. S. A.* **110**, E2544–E2551 (2013). DOI 10.1073/pnas.1301664110.

15. Rosko, J., Martinez, V., Poon, W. & Pilizota, T. Osmotaxis in Escherichia coli through changes in motor speed. *Proc. Natl. Acad. Sci. U. S. A.* **114**, E7969–E7976 (2017). DOI 10.1073/pnas.1620945114. 1703.03926.

16. Krasnopeeva, E. *Single cell measurements of bacterial physiology traits during exposure to an external stress*. Ph.D. thesis, The University of Edinburgh (2018).

17. Pilizota, T. & Shaevitz, J. W. Fast, multiphase volume adaptation to hyperosmotic shock by Escherichia coli. *PLoS One* **7**, e35205 (2012). DOI 10.1371/journal.pone.0035205.

18. Meyer, R. L. *et al.* Immobilisation of living bacteria for AFM imaging under physiological conditions. *Ultramicroscopy* (2010). DOI 10.1016/j.ultramic.2010.06.010.

19. Sydor, A. M., Czymmek, K. J., Puchner, E. M. & Mennella, V. Super-Resolution Microscopy: From Single Molecules to Supramolecular Assemblies. *Trends Cell Biol.* **25**, 730–748 (2015). DOI 10.1016/j.tcb.2015.10.004.

20. Coltharp, C. & Xiao, J. Superresolution microscopy for microbiology. *Cell. Microbiol.* **14**, 1808–1818 (2012).

21. Pilizota, T. & Shaevitz, J. Plasmolysis and cell shape depend on solute outer-membrane permeability during hyperosmotic shock in e. coli. *Biophys. J.* **104**, 2733 – 2742 (2013). URL http://www.sciencedirect.com/science/article/pii/S0006349513005614. DOI https://doi.org/10.1016/j.bpj.2013.05.011.

22. Buda, R. *et al.* Dynamics of escherichia coli's passive response to a sudden decrease in external osmolarity. *Proc. Natl. Acad. Sci.* **113**, E5838–E5846 (2016). URL https://www.pnas.org/content/113/40/E5838. DOI 10.1073/pnas.1522185113. https://www.pnas.org/content/113/40/E5838.full.pdf.

23. Tipping, M. J., Steel, B. C., Delalez, N. J., Berry, R. M. & Armitage, J. P. Quantification of flagellar motor stator dynamics through in vivo proton-motive force control. *Mol. Microbiol.* **87**, 338–347 (2013). URL https://groups.physics.ox.ac.uk/molecularmotors/pdfsofpapers/MolMicroTippingpRPMFstators.pdf. DOI 10.1111/mmi.12098.

24. Kapanidis, A. N., Uphoff, S. & Stracy, M. Understanding protein mobility in bacteria by tracking single molecules. *J. Mol. Biol.* **430**, 4443 – 4455 (2018). URL http://www.sciencedirect.com/science/article/pii/S0022283618303905. DOI https://doi.org/10.1016/j.jmb.2018.05.002. Plasticity of Multi-Protein Complexes.

25. Parry, B. R. *et al.* The bacterial cytoplasm has glass-like properties and is fluidized by metabolic activity. *Cell* **156**, 183–194 (2014). DOI 10.1016/j.cell.2013.11.028. NIHMS150003.

26. Munder, M. C. *et al.* A pH-driven transition of the cytoplasm from a fluid- to a solid-like state promotes entry into dormancy. *Elife* **5** (2016). DOI 10.7554/eLife.09347.

27. Cowan, S. E., Liepmann, D. & Keasling, J. D. Development of engineered biofilms on poly- l-lysine patterned surfaces. *Biotechnol. Lett.* **23**, 1235–1241 (2001). URL https://doi.org/10.1023/A:1010581503842. DOI 10.1023/A:1010581503842.

28. Touhami, A., Jericho, M. H., Boyd, J. M. & Beveridge, T. J. Nanoscale characterization and determination of adhesion forces of Pseudomonas aeruginosa pili by using atomic force microscopy. *J. Bacteriol.* **188**, 370–377 (2006). URL http://www.ncbi.nlm.nih.gov/pubmed/16385026http://www.pubmedcentral.nih.gov/articlerender.fcgi?artid=PMC1347306. DOI 10.1128/JB.188.2.370-377.2006.

29. Katsu, T., Tsuchiya, T. & Fujita, Y. Dissipation of membrane potential of Escherichia coli cells induced by macromolecular polylysine. *Biochem. Biophys. Res. Commun.* **122**, 401–6 (1984).

30. Colville, K., Tompkins, N., Rutenberg, A. D. & Jericho, M. H. Effects of poly(L-lysine) substrates on attached Escherichia coli bacteria. *Langmuir* **26**, 2639–2644 (2010). DOI 10.1021/la902826n.

31. Conte, M., Aliberti, F., Fucci, L. & Piscopo, M. Antimicrobial activity of various cationic molecules on foodborne pathogens. *World J. Microbiol. Biotechnol.* **23**, 1679–1683 (2007). URL http://link.springer.com/10.1007/s11274-007-9415-6. DOI 10.1007/s11274-007-9415-6.

32. Bakshi, S., Siryaporn, A., Goulian, M. & Weisshaar, J. C. Superresolution imaging of ribosomes and RNA polymerase in live Escherichia coli cells. *Mol. Microbiol.* **85**, 21–38 (2012).

33. Mohapatra, S., Choi, H., Ge, X., Sanyal, S. & Weisshaar, J. C. Spatial Distribution and Ribosome-Binding Dynamics of EF-P in Live Escherichia coli. *MBio* **8**, e00300–17 (2017).

34. Wang, S., Arellano-Santoyo, H., Combs, P. a. & Shaevitz, J. W. Measuring the bending stiffness of bacterial cells using an optical trap. *J. Vis. Exp.* 8–9 (2010). DOI 10.3791/2012.

35. Dickson, J. S. & Koohmaraie, M. Cell surface charge characteristics and their relationship to bacterial attachment to meat surfaces. *Appl. Environ. Microbiol.* **55**, 832–836 (1989). URL http://aem.asm.org/.

36. Sowa, Y. *et al.* Direct observation of steps in rotation of the bacterial flagellar motor. *Nat.* **437**, 916–919 (2005). URL http://www.nature.com/articles/nature04003. DOI 10.1038/nature04003.

37. Pilizota, T. *et al.* A molecular brake, not a clutch, stops the rhodobacter sphaeroides flagellar motor. *Proc. Natl. Acad. Sci.* **106**, 11582–11587 (2009). URL https://www.pnas.org/content/106/28/11582. DOI 10.1073/pnas.0813164106. https://www.pnas.org/content/106/28/11582.full.pdf.

38. Sowa, Y. & Berry, R. M. Bacterial flagellar motor. *Q. Rev. Biophys.* **41**, 103–132 (2008). URL https://groups.physics.ox.ac.uk/molecularmotors/pdfsofpapers/QRBSowaBFMreview2008.pdf. DOI 10.1017/S0033583508004691.

39. Waite, J. H. & Tanzer, M. L. Polyphenolic substance of Mytilus edulis: Novel adhesive containing L-dopa and hydroxyproline. *Sci. (80-.).* **212**, 1038–1040 (1981). DOI 10.1126/science.212.4498.1038.

40. Papov, V. V., Diamond, T. V., Biemann, K. & Waite, J. H. Hydroxyarginine-containing polyphenolic proteins in the adhesive plaques of the marine mussel Mytilus edulis. *J. Biol. Chem.* **270**, 20183–20192 (1995). DOI 10.1074/jbc.270.34.20183. arXiv:1011.1669v3.

41. Lee, B. P., Messersmith, P., Israelachvili, J. & Waite, J. Mussel-inspired adhesives and coatings. *Annu. Rev. Mater. Res.* **41**, 99–132 (2011). URL https://doi.org/10.1146/annurev-matsci-062910-100429. DOI 10.1146/annurev-matsci-062910-100429. https://doi.org/10.1146/annurev-matsci-062910-100429.

42. Gokaltun, A., Yarmush, M. L., Asatekin, A. & Usta, O. B. Recent advances in nonbiofouling PDMS surface modification strategies applicable to microfluidic technology. *TECHNOLOGY* **05**, 1–12 (2017). URL http://www.ncbi.nlm.nih.gov/pubmed/28695160http://www.pubmedcentral.nih.gov/articlerender.fcgi?artid=PMC5501164. DOI 10.1142/s2339547817300013.

43. Harris, L. K. & Theriot, J. A. Surface Area to Volume Ratio: A Natural Variable for Bacterial Morphogenesis. *Trends Microbiol.* **26**, 815–832 (2018). URL http://www.ncbi.nlm.nih.gov/pubmed/29843923http://www.pubmedcentral.nih.gov/articlerender.fcgi?artid=PMC6150810. DOI 10.1016/j.tim.2018.04.008.

44. Gorden, J. & Small, P. L. Acid resistance in enteric bacteria. *Infect. Immun.* **61**, 364–7 (1993).

45. Lin, J., Lee, I. S., Frey, J., Slonczewski, J. L. & Foster, J. W. Comparative analysis of extreme acid survival in Salmonella typhimurium, Shigella flexneri, and Escherichia coli. *J. Bacteriol.* **177**, 4097–4104 (1995). DOI 10.1128/jb.177.14.4097-4104.1995.

46. Slonczewski, J. L., Fujisawa, M., Dopson, M. & Krulwich, T. A. Cytoplasmic pH Measurement and Homeostasis in Bacteria and Archaea. *Adv. Microb. Physiol.* **55** (2009). DOI 10.1016/S0065-2911(09)05501-5.

47. Zilberstein, D., Agmon, V., Schuldiner, S. & Padan, E. Escherichia coli intracellular pH, membrane potential, and cell growth. *J. Bacteriol.* **158**, 246–252 (1984).

48. Slonczewski, J. L., Rosen, B. P., Alger, J. R. & Macnab, R. M. pH homeostasis in Escherichia coli: measurement by 31P nuclear magnetic resonance of methylphosphonate and phosphate. *Proc. Natl. Acad. Sci. U. S. A.* **78**, 6271–6275 (1981). DOI 10.1073/pnas.78.10.6271.

49. Lund, P., Tramonti, A. & De Biase, D. Coping with low pH: Molecular strategies in neutralophilic bacteria. *FEMS Microbiol. Rev.* **38**, 1091–1125 (2014). DOI 10.1111/1574-6976.12076.

50. Mitchell, P. Coupling of phosphorylation to electron and hydrogen transfer by a chemi-osmotic type of mechanism. *Nat.* **191**, 144–148 (1961). DOI 10.1038/191144a0.

51. Bearne, S. L. Illustrating the effect of pH on enzyme activity using Gibbs energy profiles. *J. Chem. Educ.* **91**, 84–90 (2014). DOI 10.1021/ed400229g.

52. Martinez, K. A. *et al.* Cytoplasmic pH response to acid stress in individual cells of Escherichia coli and Bacillus subtilis observed by fluorescence ratio imaging microscopy. *Appl. Environ. Microbiol.* **78**, 3706–3714 (2012). DOI 10.1128/AEM.00354-12.

53. Chakraborty, S., Winardhi, R. S., Morgan, L. K., Yan, J. & Kenney, L. J. Non-canonical activation of OmpR drives acid and osmotic stress responses in single bacterial cells. *Nat. Commun.* **8**, 1587 (2017). DOI 10.1038/s41467-017-02030-0.

54. Miller, S. I., Kukral, A. M. & Mekalanos, J. J. A two-component regulatory system (phoP phoQ) controls Salmonella typhimurium virulence. *Proc. Natl. Acad. Sci. U. S. A.* **86**, 5054–5058 (1989). DOI 10.1073/pnas.86.13.5054.

55. Choi, J. & Groisman, E. A. Acidic pH sensing in the bacterial cytoplasm is required for Salmonella virulence. *Mol. Microbiol.* **101**, 1024–1038 (2016). DOI 10.1111/mmi.13439.

56. Morimoto, Y. V., Kojima, S., Namba, K. & Minamino, T. M153R mutation in a pH-sensitive green fluorescent protein stabilizes its fusion proteins. *PLoS One* **6**, e19598 (2011). DOI 10.1371/journal.pone.0019598.

57. Krasnopeeva, E., Lo, C.-J. & Pilizota, T. Single-cell bacterial electrophysiology reveals mechanisms of stress-induced damage. *Biophys. J.* **0** (2019). URL https://linkinghub.elsevier.com/retrieve/pii/S0006349519303923http://arxiv.org/abs/1809.05306. DOI 10.1016/j.bpj.2019.04.039. 1809.05306.

58. Wilks, J. C. *et al.* Acid and base stress and transcriptomic responses in bacillus subtilis. *Appl. Environ. Microbiol.* **75**, 981–990 (2009). URL https://aem.asm.org/content/75/4/981. DOI 10.1128/AEM.01652-08. https://aem.asm.org/content/75/4/981.full.pdf.

59. Zarkan, A. *et al.* Indole Pulse Signalling Regulates the Cytoplasmic pH of E. coli in a Memory-Like Manner. *Sci. Rep.* **9**, 3868 (2019). URL http://www.nature.com/articles/s41598-019-40560-3. DOI 10.1038/s41598-019-40560-3.

60. Wallden, M., Fange, D., Lundius, E. G., Özden Baltekin & Elf, J. The synchronization of replication and division cycles in individual e. coli cells. *Cell* **166**, 729 – 739 (2016). URL http://www.sciencedirect.com/science/article/pii/S0092867416308601. DOI https://doi.org/10.1016/j.cell.2016.06.052.

61. Thomas, P., Terradot, G., Danos, V. & Weiße, A. Y. Sources, propagation and consequences of stochasticity in cellular growth. *Nat. Commun.* **9**, 4528 (2018). URL http://www.nature.com/articles/s41467-018-06912-9. DOI 10.1038/s41467-018-06912-9.

62. Osella, M., Nugent, E. & Cosentino Lagomarsino, M. Concerted control of Escherichia coli cell division. *Proc. Natl. Acad. Sci. U. S. A.* **111**, 3431–5 (2014). DOI 10.1073/pnas.1313715111.

63. Campos, M. *et al.* A constant size extension drives bacterial cell size homeostasis. *Cell* **159**, 1433–1446 (2014). DOI 10.1016/j.cell.2014.11.022. NIHMS150003.

64. Beloin, C., Roux, A. & Ghigo, J. M. Escherichia coli biofilms. *Curr. Top. Microbiol. Immunol.* **322**, 249–89 (2008). URL http://www.ncbi.nlm.nih.gov/pubmed/18453280http://www.pubmedcentral.nih.gov/articlerender.fcgi?artid=PMC2864707http://www.ncbi.nlm.nih.gov/pubmed/18453280{%}0Ahttp://www.pubmedcentral.nih.gov/articlerender.fcgi?artid=PMC2864707.

65. Ellison, C. K. *et al.* Obstruction of pilus retraction stimulates bacterial surface sensing. *Sci.* **358**, 535–538 (2017). URL https://science.sciencemag.org/content/358/6362/535. DOI 10.1126/science.aan5706. https://science.sciencemag.org/content/358/6362/535.full.pdf.

66. Cattoni, D. I., Fiche, J. B., Valeri, A., Mignot, T. & Nöllmann, M. Super-Resolution Imaging of Bacteria in a Microfluidics Device. *PLoS ONE* **8** (2013). DOI 10.1371/journal.pone.0076268.

67. Griffith, J. M. *et al.* Experimental evolution of escherichia coli k-12 in the presence of proton motive force (pmf) uncoupler carbonyl cyanide m-chlorophenylhydrazone selects for mutations affecting pmf-driven drug efflux pumps. *Appl. Environ. Microbiol.* **85** (2019). URL https://aem.asm.org/content/85/5/e02792-18. DOI 10.1128/AEM.02792-18. https://aem.asm.org/content/85/5/e02792-18.full.pdf.

68. Bennett, B. D. *et al.* Absolute metabolite concentrations and implied enzyme active site occupancy in Escherichia coli. *Nat. Chem. Biol.* **5**, 593–599 (2009). DOI 10.1038/nchembio.186.Absolute.

69. Kitko, R. D. *et al.* Cytoplasmic acidification and the benzoate transcriptome in bacillus subtilis. *PLOS ONE* **4**, 1–12 (2009). URL https://doi.org/10.1371/journal.pone.0008255. DOI 10.1371/journal.pone.0008255.

70. Lazar, S. W., Almirón, M., Tormo, A. & Kolter, R. Role of the Escherichia coli SurA protein in stationary-phase survival. *J. Bacteriol.* **180**, 5704–5711 (1998). DOI D - NLM: PMC107631 EDAT- 1998/10/29 MHDA- 1998/10/29 00:01 CRDT- 1998/10/29 00:00 PST - ppublish.

71. Molina, P. M., Parma, A. E. & Sanz, M. E. Survival in acidic and alcoholic medium of Shiga toxin-producing Escherichia coli O157:H7 and non-O157:H7 isolated in Argentina. *BMC Microbiol.* **3**, 1–6 (2003). DOI 10.1186/1471-2180-3-17.

72. Kuwajima, G. Construction of a minimum-size functional flagellin of Escherichia coli. *J. Bacteriol.* **170**, 3305–3309 (1988). DOI 10.1128/jb.170.7.3305-3309.1988.

73. Yao, Z., Kahne, D. & Kishony, R. Distinct Single-Cell Morphological Dynamics under Beta-Lactam Antibiotics. *Mol. Cell* **48**, 705–712 (2012). URL http://www.ncbi.nlm.nih.gov/pubmed/23103254http://www.pubmedcentral.nih.gov/articlerender.fcgi?artid=PMC3525771. DOI 10.1016/j.molcel.2012.09.016.

74. Fletcher, E., Pilizota, T., Davies, P. R., McVey, A. & French, C. E. Characterization of the effects of n-butanol on the cell envelope of E. coli. *Appl. Microbiol. Biotechnol.* **100**, 9653–9659 (2016). URL http://link.springer.com/10.1007/s00253-016-7771-6. DOI 10.1007/s00253-016-7771-6.

75. Schindelin, J. *et al.* Fiji: an open-source platform for biological-image analysis. *Nat. methods* **9**, 676 (2012).

76. Meyer, F. & Beucher, S. Morphological segmentation. *J. Vis. Commun. Image Represent.* **1**, 21–46 (1990). URL https://doi.org/10.1016/1047-3203(90)90014-m. DOI 10.1016/1047-3203(90)90014-m.

77. Soille, P. *Morphological image analysis: principles and applications* (Springer Science & Business Media, 1999).

78. Legland, D., Arganda-Carreras, I. & Andrey, P. MorphoLibJ: integrated library and plugins for mathematical morphology with ImageJ. *Bioinforma.* btw413 (2016). URL https://doi.org/10.1093/bioinformatics/btw413. DOI 10.1093/bioinformatics/btw413.

79. Guberman, J. M., Fay, A., Dworkin, J., Wingreen, N. S. & Gitai, Z. PSICIC: Noise and asymmetry in bacterial division revealed by computational image analysis at sub-pixel resolution. *PLoS Comput. Biol.* **4** (2008). DOI 10.1371/journal.pcbi.1000233.

80. Moré, J. The levenberg-marquardt algorithm: Implementation and theory. In Watson, G. (ed.) *Numerical Analysis*, vol. 630 of *Lecture Notes in Mathematics*, 105–116 (Springer Berlin Heidelberg, 1978). URL http://dx.doi.org/10.1007/BFb0067700. DOI 10.1007/BFb0067700.

81. Jones, E., Oliphant, T., Peterson, P. *et al.* SciPy: Open source scientific tools for Python (2001–). URL http://www.scipy.org/.

82. Chimerel, C., Field, C. M., Piñero-Fernandez, S., Keyser, U. F. & Summers, D. K. Indole prevents Escherichia coli cell division by modulating membrane potential. *Biochim. Biophys. Acta - Biomembr.* **1818**, 1590–1594 (2012). DOI 10.1016/j.bbamem.2012.02.022.

Acknowledgements

This project is supported by the Human Frontier Science Program Grant (RGP0041/2015) to TP, CJL and FB. CJL is financially supported by the Ministry of Science and Technology, Republic of China under contract No. MOST-107-2112-M-008-025-MY3. EK was supported by the Global Research and Principal's Career Development PhD Scholarships. We thank Tom Shimizu and Victor Caldas (AMOLF) for sharing the APTES protocol of immobilization.

Author contributions statement

YKW, EK, FB, TP and CJL designed research. YKW and EK performed research and analysed data. YKW, EK, FB, TP and CJL interpreted results and wrote the paper. All authors reviewed the manuscript.

Supplementary Materials

Supplementary Methods: pHluorin calibration

The *in vivo* calibration of pH sensor was performed as follows[16]. The mixture of 100 mM MES, HEPES and AMPSO buffers was adjusted to a set of pH values in the range between 5.5 and 9, and supplemented with one of the three pH collapsing agents: 40 mM potassium benzoate and 40 mM methylamine hydrochloride (PBMH)[52], 25 µM CCCP or 5 mM indole[82]. Tunnel-slides were prepared as previously described[16,57]: two bits of sticky tape form a tunnel and are sandwiched between a coverslip and a microscope slide. Buffer of known pH was flushed into a channel, incubated for 15 min, upon which 5 different fields of view containing over 100 cells were imaged with 50 ms exposure time. The calibration curves were plotted as ratio of emission intensities for excitation at 395 nm and 475 nm against pH, and fitted with the sigmoid function $R_{395/475} = (a_1 e^{k(pH-pH_0)} + a_2)/(e^{k(pH-pH_0)} + 1)$, where a_1, a_2, k and pH_0 are free fitting parameters.

In vitro calibration was performed with the purified pHluorin protein diluted into buffer of known pH in the 96-well plate (Thermo Scientific, Optical bottom). The pHluorin excitation spectra for 510 nm emission was measured in Spark 10M multimode plate reader (Tecan Trading AG, Switzerland). The His-tagged protein was purified using affinity chromatography column[16]. The excitation spectra was scanned from 380 nm to 480 nm with 5 nm step size. Additionally, the autofluorescence of the buffer with no added protein was measured and subtracted from the measured protein intensity.

Supplementary Figures

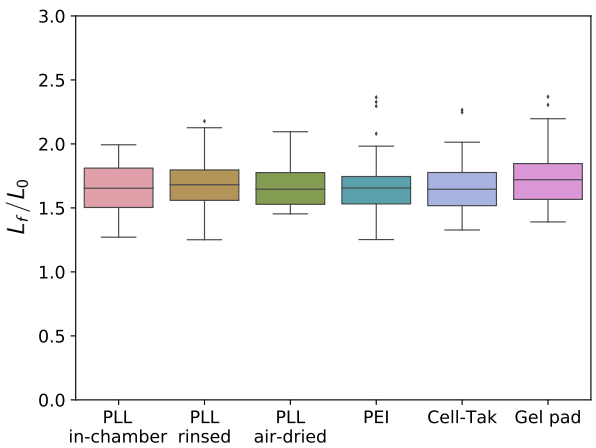

SI Figure 1. Final length to the initial length ratio (L_f/L_0) stays constant when cells are attached to the surface with different immobilization methods. L_0 is the length after the first division, and L_f the length before the second division.

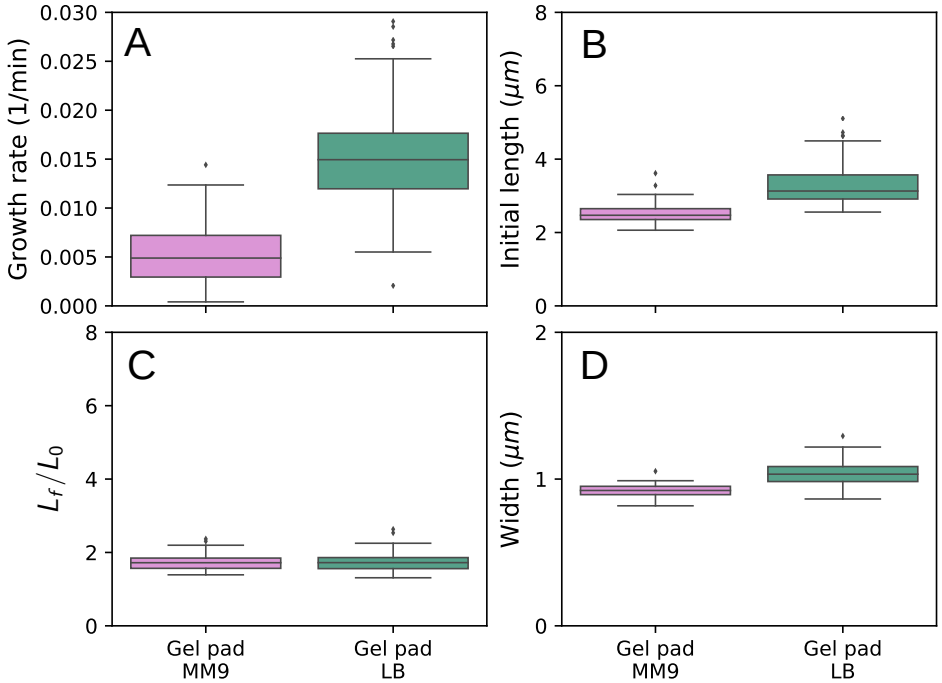

SI Figure 2. Comparison of (**A**) the growth rate, (**B**) initial cell length L_0, (**C**) length ratio L_f/L_0 and (**D**) cell width for cells growing on the gel pad in MM9 and LB media.

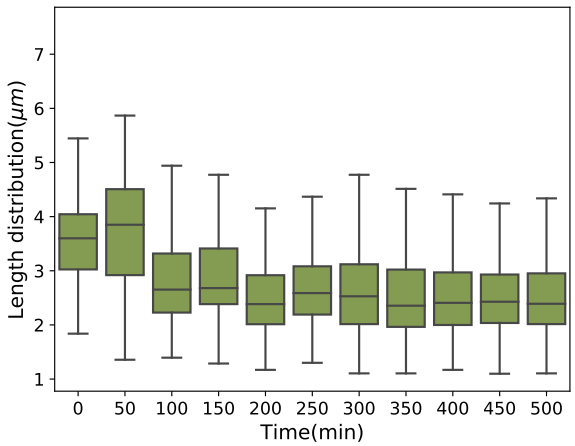

SI Figure 3. Cell length distribution over time on the PLL air-dried surface. The average length of the cells population changes from 3.53 ± 0.92 µm to 2.53 ± 0.74 µm. A steady length distribution is reached by the second generation of surface-grown bacteria with the mean being roughly 28% smaller than that of the liquid cultured bacteria.

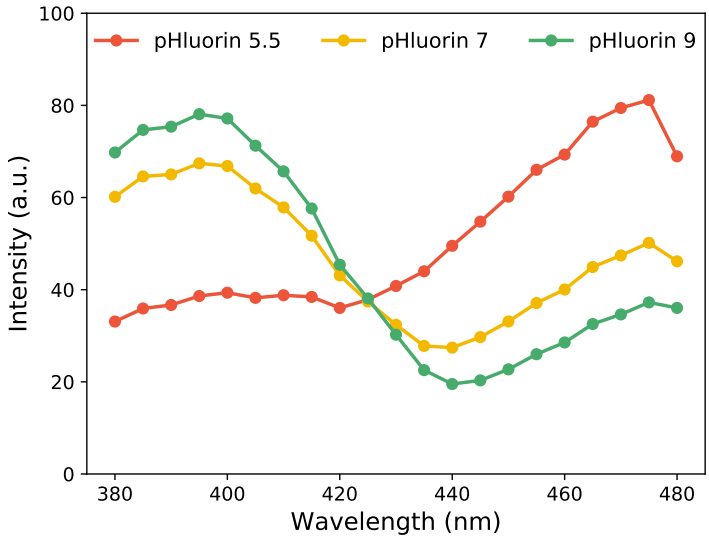

SI Figure 4. Excitation spectra of purified pHluorin at pH values 5.5 (red), 7.0 (yellow) and 9.0 (green). Emission is collected at 510 nm.

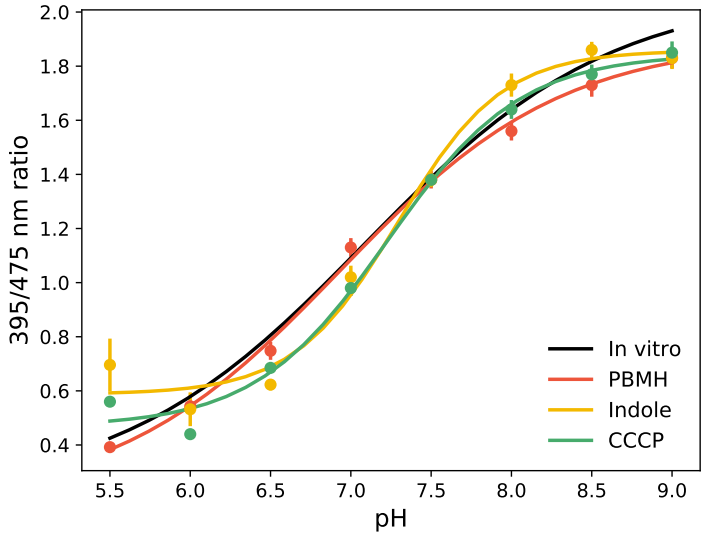

SI Figure 5. Comparison of the *in vivo* and *in vitro* calibration curves. Coloured lines show *in vivo* pHluorin calibration curves with 40 mM PBMH (red), 5 mM indole (yellow) or 25 μM CCCP (green) as ΔpH collapsing agents. Black curve shows *in vitro* calibration curve of purified pHluorin in buffer with no supplements. *In vivo* curve with PMBH aligns best with the *in vitro* curve.

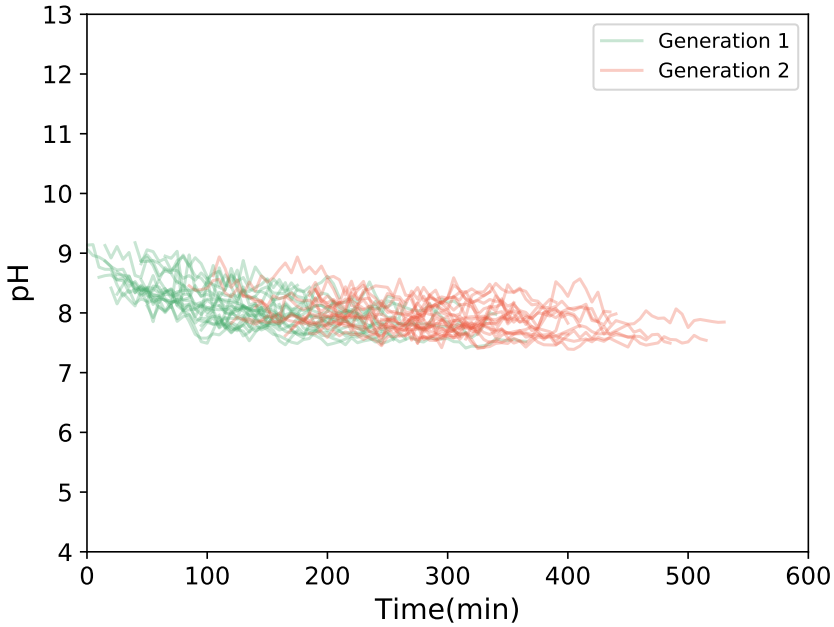

SI Figure 6. Single cell intracellular pH dynamics for two generations of bacteria, first generation is shown in green and the second in red. Cells are grown on the PLL ”in-chamber” coated surface.

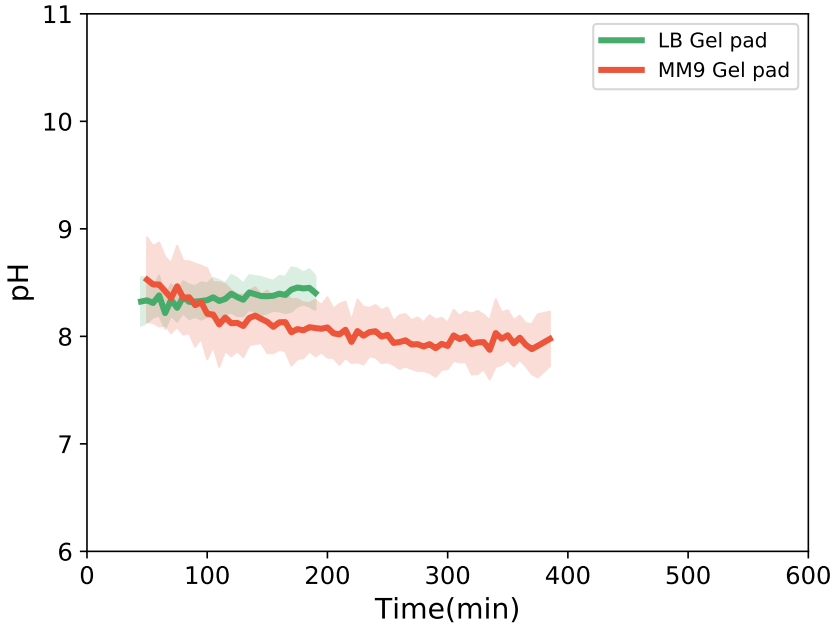

SI Figure 7. Mean and the standard deviation of the intracellular pH of the cells grown in the gel pad in LB (green) or MM9 (red) media.

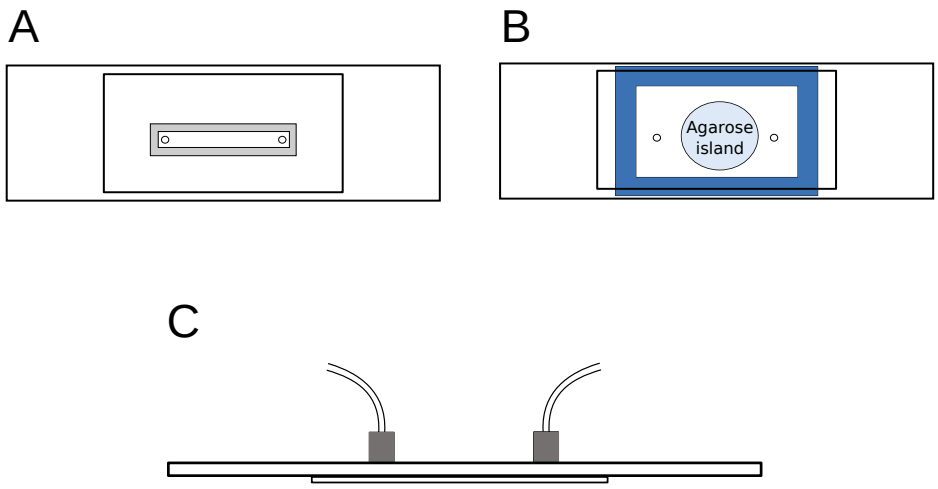

SI Figure 8. Schematic of our flow chambers for bacterial immobilsation experiments. (**A**) top view of the flow chamber used for surface attachments, (**B**) top view of chamber for agarose island experiments, and (**C**) side view of flow chambers.